

# Diffraction-Based Density Restraints for Membrane and Membrane-Peptide Molecular Dynamics Simulations

Ryan W. Benz,\* Hirsh Nanda,<sup>†‡</sup> Francisco Castro-Román,<sup>†</sup> Stephen H. White,<sup>†</sup> and Douglas J. Tobias\*

\*Department of Chemistry, and <sup>†</sup>Department of Physiology and Biophysics, University of California, Irvine, California; and <sup>‡</sup>NIST Center for Neutron Research, National Institute of Standards and Technology, Gaithersburg, Maryland

**ABSTRACT** We have recently shown that current molecular dynamics (MD) atomic force fields are not yet able to produce lipid bilayer structures that agree with experimentally-determined structures within experimental errors. Because of the many advantages offered by experimentally validated simulations, we have developed a novel restraint method for membrane MD simulations that uses experimental diffraction data. The restraints, introduced into the MD force field, act upon specified groups of atoms to restrain their mean positions and widths to values determined experimentally. The method was first tested using a simple liquid argon system, and then applied to a neat dioleoylphosphatidylcholine (DOPC) bilayer at 66% relative humidity and to the same bilayer containing the peptide melittin. Application of experiment-based restraints to the transbilayer double-bond and water distributions of neat DOPC bilayers led to distributions that agreed with the experimental values. Based upon the experimental structure, the restraints improved the simulated structure in some regions while introducing larger differences in others, as might be expected from imperfect force fields. For the DOPC-melittin system, the experimental transbilayer distribution of melittin was used as a restraint. The addition of the peptide caused perturbations of the simulated bilayer structure, but which were larger than observed experimentally. The melittin distribution of the simulation could be fit accurately to a Gaussian with parameters close to the observed ones, indicating that the restraints can be used to produce an ensemble of membrane-bound peptide conformations that are consistent with experiments. Such ensembles pave the way for understanding peptide-bilayer interactions at the atomic level.

## INTRODUCTION

X-ray and neutron diffraction are commonly used for studying the structure of membrane systems (1–3). In these experiments, a set of discrete structure factors is measured that represents the reciprocal-space structure of the membrane. Typically, only 4–10 orders of diffraction (i.e., structure factors) are observable due to the high degree of thermal disorder present in fluid membranes (4). Inversion of the structure factors via Fourier transformation yields a real-space density profile, which can be interpreted as a 1D electron or neutron scattering-length density projected along the bilayer normal (5). These profiles represent the time-averaged, transmembrane structure of the membrane. Although these profiles are useful for many purposes, they cannot by themselves provide unambiguous atomic-level information about the distribution of the molecular components underlying the profile (6). Molecular dynamics simulations used in concert with experimental data offer the possibility of supplying the missing atomic-level information (7).

Some of the missing information can be obtained using x-ray or neutron diffraction by specifically labeling lipid component groups with heavy atoms, such as bromine (8,9) for x-rays or deuterons (10,11) for neutrons. This labeling

allows the component groups to be highlighted within the profile structure. Subtraction of the scattering-length density profile of the unlabeled membrane from the specifically labeled one yields a so-called difference-structure profile, which reveals the transbilayer distribution of the labeled group, provided that the labeling does not change the structure of the system (isomorphous replacement) (11).

Component group distributions give information about where a particular group is located in the bilayer, the extent to which the atoms in the group visit other regions of the bilayer, and the degree of the thermal fluctuations (4). Component group distributions can often (but not always) be accurately modeled as Gaussians, parameterized by distribution means and widths (6,11,12). By means of the joint-refinement of x-ray and neutron data, the complete structure of only one bilayer (dioleoylphosphatidylcholine (DOPC) at 66% relative humidity (RH)) has been solved thus far. The structure is comprised of a set of Gaussian parameters for each of eight component groups in the system (water, double-bond, terminal methyl, methylene, carbonyl, glycerol, phosphate, and choline) (6). Although knowledge of the complete structure of a bilayer is quite useful, it is exceedingly difficult to achieve in practice, particularly for membranes at full hydration. Nevertheless, determination of the distribution of even one or two component groups can provide a great deal of structural information that can be helpful for guiding other methods, such as computer simulations.

This approach can also be used for bilayers containing specifically labeled peptides (13,14). Another approach for

*Submitted March 6, 2006, and accepted for publication August 9, 2006.*

Address reprint requests to Douglas J. Tobias, E-mail: dtobias@uci.edu; or Stephen H. White, E-mail: stephen.white@uci.edu.

Francisco Castro-Román's present address is Departamento de Física, Centro de Investigación y Estudios Avanzados del Instituto Politécnico Nacional, A.P. 14-740, México Distrito Federal, Zacatenco CP 07360, México.

© 2006 by the Biophysical Society

0006-3495/06/11/3617/13 \$2.00

doi: 10.1529/biophysj.106.084483

determining the transbilayer distribution of peptides is the so-called absolute-scale refinement method (15,16). Using this approach, Hristova et. al. (16) determined the disposition of monomeric melittin (MLT) in DOPC bilayers via x-ray diffraction measurements. Because the low concentration of MLT did not strongly perturb the bilayer structure, it was possible to model the peptide-perturbed bilayer from changes in the transbilayer distribution of bromine-labeled DOPC double-bonds. However, at higher concentrations of MLT, the perturbations to the bilayer were too large to be modeled by a simple perturbation approach.

In principle, MD simulations of melittin in DOPC could have been used to determine the structure of the peptide-perturbed bilayer and to create an ensemble of peptide conformations consistent with the experimental data. With this goal in mind, we have developed a novel restraint potential for use in molecular dynamics (MD) simulations based upon diffraction data obtained from membranes. Restraint potentials have been used frequently in molecular simulations for a variety of purposes, including NMR structure refinement (17–19) and free-energy calculations (20–22). The restraints presented here for use in MD simulations of lipid bilayers and bilayer-peptide systems are based upon component group distribution parameters obtained directly from diffraction experiments. Unlike other lipid bilayer structural parameters, such as the molecule area/lipid, which can only be determined indirectly from diffraction experiments (23), component group distributions obtained via isomorphous labeling are direct measurements, and therefore can be treated with a high degree of certainty.

The diffraction-based restraints described here are used to restrain a given group of atoms such that they adopt a specified mean position and width determined from the experimentally determined Gaussian distributions, effectively allowing the restrained components to sample configurations consistent with experimental data. To test the approach, restraints were used on three different test systems: a box of liquid argon, a DOPC bilayer at 66% RH (5.4 waters/lipid), and a DOPC bilayer at 66% RH containing melittin at a concentration of 0.015 peptides/lipid. We describe below the results of the application of the restraint procedure to these three systems.

## METHODS

### Diffraction-based restraint potential

To restrain the mean position and width of a collection of atoms in accordance with experimentally determined Gaussian distributions, a two-term, harmonic potential is used:

$$V(Z, \sigma) = K_z(Z - Z^*)^2 + K_\sigma(\sigma - \sigma^*)^2. \quad (1)$$

In Eq. 1,  $Z$  and  $\sigma$  are instantaneous group distribution mean position and standard deviation, respectively, and,  $K_z$  and  $K_\sigma$  are the corresponding force constants. The values,  $Z^*$  and  $\sigma^*$  represent the target values for the restraint, which, for our method, are taken from the experimentally determined Gaussian distribution parameters obtained from the refinement of diffraction

data. Because diffraction data provide information only about transmembrane structure, the potential is defined in terms of the transmembrane positional components of the atoms (i.e., the  $z$ -component of the group mean and standard deviation). At each step during the course of the simulation, the instantaneous mean position  $Z$  and standard deviation  $\sigma$  are calculated for each restraint group according to

$$Z = \frac{\sum_{i=1}^n z_i}{n}, \quad (2)$$

and

$$\sigma = \sqrt{\frac{\sum_{i=1}^n (z_i - Z)^2}{n - 1}}. \quad (3)$$

A force

$$F_i = -\frac{\partial V}{\partial z_i} = -\frac{\partial V_z}{\partial z_i} - \frac{\partial V_\sigma}{\partial z_i}, \quad (4)$$

is applied to each atom in the group. In this expression,

$$\frac{\partial V_z}{\partial z_i} = \frac{2K_z(Z - Z^*)}{n}, \quad (5)$$

$$\frac{\partial V_\sigma}{\partial z_i} = \frac{2K_\sigma(z_i - Z)(\sigma - \sigma^*)}{(n - 1)\sigma}, \quad (6)$$

$V_z$  is the first term and  $V_\sigma$  the second term in Eq. 1,  $z_i$  indicates the position  $z$ -component for atom  $i$ , and  $n$  is the total number of atoms in the restraint group. Although distribution parameters for a given group are specified by one set of values (a mean position and width), in practice, one must use two restraints to restrain a single group, one for each leaflet, which have the same parameters except for differing signs on  $Z^*$ .

## Simulations

All simulations were run using the NAMD molecular dynamics package (24) version 2.5 and the CHARMM27 force field (25–27) in the NPT ensemble (constant particle number, pressure, and temperature), except for the liquid argon simulation, which used standard Lennard-Jones parameters for liquid argon (28) ( $\epsilon/kb = 119.8$  K,  $\sigma = 0.341$  nm) and run at NVT conditions (constant particle number, volume, and temperature). In addition, as a control, the “neat” (peptide-free) DOPC bilayer was also run under NVT conditions. For the constant-pressure simulations, the Nose-Hoover Langevin piston method (29,30) was used with a target pressure of 1.0 bar and a fully flexible, orthorhombic cell. Langevin dynamics was used to control the temperature, at 94.4 K for the liquid argon system and 296 K for the bilayer and bilayer-MLT systems. The electrostatic contributions were calculated using the smooth particle-mesh Ewald summation method (31), and the van der Waals interactions were switched smoothly to zero from 10–11 Å. A neighbor list, updated every eight steps, was used for the nonbonded interactions with a radius of 12.5 Å. Multiple time-stepping was used via the impulse-based Verlet-I/r-RESPA method (32,33) with a 1-fs step for the bonded interactions, 2 fs for the short-range nonbonded interactions, and 4 fs for the long-range electrostatic interactions. For the NVT simulation of the neat DOPC bilayer, the experimental repeat distance or  $d$ -spacing (49.1 Å) and area/lipid (59.3 Å<sup>2</sup>) values were used to define the cell dimensions (6). The molecular graphics shown in the article were produced using VMD (34).

## Systems

Three different systems were used to test the diffraction-based restraint potential: 1), a box of liquid argon; 2), a pure DOPC bilayer at 66% RH; and 3), a DOPC bilayer at 66% RH containing MLT. For the DOPC and DOPC-MLT systems, restraints were applied to groups for which the distribution

parameters had been determined from diffraction experiments (Table 1). As the liquid argon system was used simply to test the effectiveness of the restraints, arbitrary restraint parameters were used. The restrained groups and the corresponding parameters used are summarized in Table 1, with more detail on the individual systems described below. Although pure DOPC bilayers (7,26,35) and melittin in a membrane environment (36–39) have previously been simulated, the restrained simulations reported here show how experimental diffraction data can be used to help guide membrane and membrane/protein simulations.

### Liquid argon

A cube of 864 argon atoms measuring  $\sim 35$  Å on a side was used to test the efficiency of the restraints. Four different restraints were applied to four groups of 216 argon atoms each, which differed in the choice of the target mean position, to separate the groups from one another. All of the restraints used the same distribution mean and standard deviation force constants of 100 and 200 kcal/mol/Å<sup>2</sup>, respectively, as well as a target-distribution standard deviation of 5.0 Å. The target mean positions were chosen to be  $-75$ ,  $-25$ ,  $25$ , and  $75$  Å from the center of the box, along the  $z$  axis. To allow the groups to separate without interference, the  $z$ -component cell dimension was increased to 200 Å.

### DOPC bilayer

The DOPC bilayer, consisting of 72 lipids (36 lipids in each leaflet) with 5.4 waters/lipid, was simulated with restraints applied on the double-bond and water component groups, using distribution parameters obtained for these groups by White and colleagues (6,9,11). The starting configuration was taken from a previous simulation (7), which was then run for several nanoseconds, during which time the restraint force constants were adjusted to allow the distribution parameters to reach the desired target mean and standard deviation values (Table 1). After this equilibration period, the simulation was run for an additional 5 ns with the restraints applied the entire time, and used for analysis. As a reference for comparison to the restrained and experimental systems, the DOPC bilayer was also simulated at NVT conditions with no restraints applied. The initial configuration was taken from the end of a previous simulation (7) and was simulated for 12 ns. The last 10 ns were used in the analyses reported below.

### DOPC bilayer with MLT

Melittin was added to the DOPC bilayer described above to test the diffraction-based restraints on a membrane protein system. Two MLT peptides with an  $\alpha$ -helical conformation were placed on the membrane water interface of each leaflet. To accommodate the MLT peptides and to produce a MLT concentration of 0.015 proteins/lipid (to match the experimental

conditions used by Hristova et al. (16)), the DOPC bilayer was replicated in the plane of the membrane to produce a system four times larger (144 lipids per leaflet). Thirteen lipids in the upper leaflet and 11 lipids in the lower leaflet were then removed to accommodate the peptides, leaving a total of 264 lipids. The MLT peptides were placed in a criss-cross pattern to maximize the distance between and to limit interaction among the proteins (Fig. 1). The peptides were oriented with hydrophobic faces of the helices oriented toward the hydrocarbon region of the membrane, determined using a helical wheel produced by the program MPEx (<http://blanco.biomol.uci.edu/mpex>). Restraints were then applied to the heavy atoms in the MLT based upon distribution parameters obtained for the peptide in the same bilayer by Hristova et al. (16), shown in Table 1. The system was run with the restraints for 12 ns with the first 6 ns representing the restraint equilibration phase. The final 6 ns were used for analysis.

## Implementation of the restraints

The restraints were implemented into NAMD (24) via the program's TCLForces interface, which allows one to easily calculate and add forces to a system during the course of a simulation through the use of scripts written in the TCL scripting language, without having to directly modify the source code. The restraint code was written into a subprocedure called "calcForces," which NAMD calls at each step. Though the simplicity of TCL makes the coding of user-defined restraints a straightforward process, TCL itself is quite slow at mathematical operations and its use can potentially add significant overhead to the simulation runtime if complex calculations are used or large numbers of atoms are restrained. For the DOPC and MLT system described below, in which 804 atoms were restrained, the restraints added negligible overhead to the calculations. For systems in which the computational overhead of the restraints becomes an issue, it is possible to wrap the main computations of the restraints into a C/C++ routine, which could then be called from the "calcForces" procedure, effectively speeding up the calculation of the restraints at each step. As of NAMD version 2.5, the pressure tensor calculation includes contributions due to applied external forces.

## RESULTS

### Liquid argon

Fig. 2 shows the initial configuration of the box of liquid argon and the final restraint-separated state, with the argon atoms colored according to which of the four restraint groups they belong to. The time evolution of the individual group mean position and standard deviation values are shown for

**TABLE 1** Restraint parameters used in the simulations

System	Restrained group	$K_z$ (kcal/mol/Å <sup>2</sup> )	$K_\sigma$ (kcal/mol/Å <sup>2</sup> )	$Z^*$ (Å)	$\sigma^*$ (Å)
Liquid argon	Group 1	100	200	$-75.0$	5.0
	Group 2	100	200	$-25.0$	5.0
	Group 3	100	200	$25.0$	5.0
	Group 4	100	200	$75.0$	5.0
Neat DOPC bilayer	Double-bond, $z > 0$	150	500	7.88	3.03
	Double-bond, $z < 0$	150	500	$-7.88$	3.03
	Water, $z > 0$	150	500	22.51	3.27
	Water, $z < 0$	150	500	$-22.51$	3.27
DOPC bilayer + MLT	MLT, $z > 0$	100	100	17.5	3.04
	MLT, $z < 0$	100	100	$-17.5$	3.04

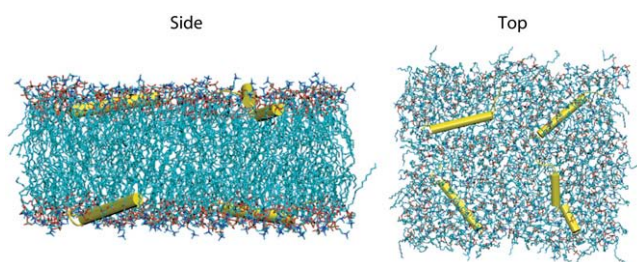


FIGURE 1 Images of the DOPC bilayer plus melittin (MLT) system taken from a frame of the molecular dynamics simulation of the system. The side view is along an axis parallel to the membrane plane. The top view is along the bilayer normal. To avoid problems that might arise from the use of periodic boundary conditions, the MLT peptides in  $\alpha$ -helical conformation were initially placed in a criss-cross pattern as shown in the top view to minimize the distance and interaction between the peptides in the two leaflets.

each restraint group in Fig. 3. It is clear for this model system that the restraints are quite effective, as all of the groups reach their target distribution values rapidly (within 40 ps of simulation time).

### Neat DOPC bilayer

The evolution of the distribution mean and width parameters for the double-bond and water groups is shown in Fig. 4. Whereas the evolution of the mean values quickly reached the target values for both the double-bond and water component groups, the standard deviation values required longer

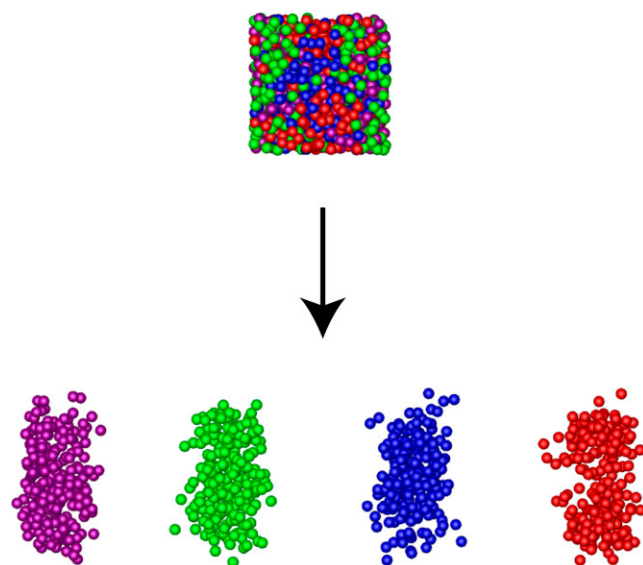


FIGURE 2 Images of the "box" of liquid argon before and after the application of the restraints (Table 1). Four restraint groups were randomly chosen throughout the box with the argon atoms colored according to group. Each group had the same distribution target width, but differed in the distribution target mean positions. After 40 ps of dynamics with the restraints, the four groups effectively separate into distinct distributions according to the restraint parameters.

times. Although Fig. 4 shows that the distribution parameters reached their target values within 6 ns, the restraint force constants were increased during this time until the target values were reached, as indicated in the figures. However, had the final force constant values (Table 1) been used initially, the system would have reached the target values much faster (within 1 ns).

To determine how the rest of the bilayer structure responded to the restrained groups, the evolution of the mean positions of headgroup component groups were computed, as shown in Fig. 5 *A* (dark blue, choline; red, phosphate; green, glycerol; light blue, carbonyl). The mean positions of the unrestrained headgroup components also evolve during the first 6 ns, at which point they reach stable values. All of the headgroup distributions show a decrease in their mean positions, indicating compression of the bilayer with the restraints applied. Fig. 5 *B* shows the evolution of the deuterium order parameters for C6 and C13 of the lipid chains. Again, the results converge after 6 ns of simulation time. Overall, these results show that the entire bilayer structure gradually evolves with the application of the restraints, and that the structure is well equilibrated after 6 ns.

Previous analysis of the same DOPC bilayer system without restraints (7) showed that several of the key molecular component groups had distribution mean and width values that differed significantly from the experimental values, including the double-bond and water groups that were restrained here. However, with restraints, the distribution parameters of these groups could be rapidly adjusted to correspond to experimental values. It is apparent from the evolution of the distribution parameters that, compared to the mean, the distribution width requires more simulation time or a larger force constant to reach the target value.

Because the total scattering-length density profile, as obtained from diffraction experiments, can be thought of as the sum of individual molecular component group distributions, restraining individual component groups to adopt the same distribution parameters should have an important effect on the underlying structure of the bilayer, especially when the unrestrained structure differs from the experimental structure. Fig. 6 *A* shows the neutron scattering-length density profiles of the restrained system compared to the experimental and unrestrained profiles that were determined previously (7). Better agreement with the experimental profile is observed in the locations of the headgroup peaks  $\sim \pm 20$  Å from the bilayer center and the peaks around the double-bond region at  $\pm 8$  Å for the restrained system, compared to the unrestrained system. Around the interfacial region ( $\pm 20$  Å), the density and width of the main peaks are better reproduced compared to the unrestrained system, in which these peaks are significantly wider and less intense. In the double-bond region ( $\pm 8$  Å), although the densities for both the restrained and unrestrained systems deviate from the experimental results, the location of the double-bond peaks and troughs are closer to the experiment for the restrained

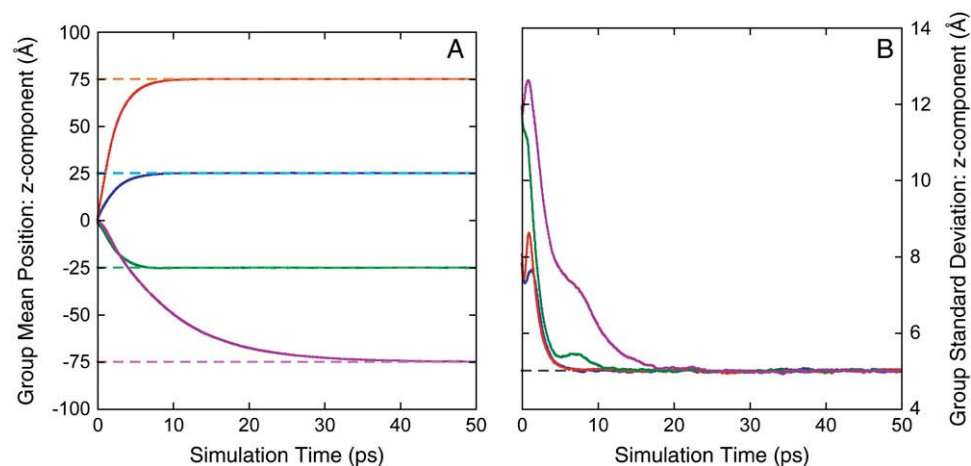


FIGURE 3 Evolution of the distribution parameters for the four restraint groups in the liquid argon example (Fig. 2). The evolution of the group mean positions and widths are shown in panels *A* and *B*, respectively. The dashed lines indicate the target values, and the solid lines, the simulation values (colored according to the scheme indicated in Fig. 2). As the center of the box was initially at the center of the simulation cell, the groups with mean restraint values closer to the center reach their respective targets more quickly. However, all of the groups rapidly reach their target restraint values within 40 ps.

system. One can also see better agreement in the restrained profile with the experimental result near the center of the bilayer.

The application of restraints to the double-bond and water component groups of the DOPC bilayer, however, does not fix all of the structural discrepancies in the simulated systems. Fig. 6 *C* shows the x-ray scattering-length density profiles for the restrained, experimental, and unrestrained systems, computed from eight orders of diffraction data. One can see that

the restraints produce structural differences compared to the experimental results. Although the location and width of the headgroup peaks at  $\pm 20$  Å from the bilayer center are close to the experimental results, the densities are clearly too high. In fact, the main discrepancies of the restrained simulations from the experiment are that the densities are generally too large in the middle region (within  $\pm 10$  Å) and the outer regions (outside of  $\pm 20$  Å) of the bilayer. These differences can be explained by considering the Bragg  $d$ -spacing distance values

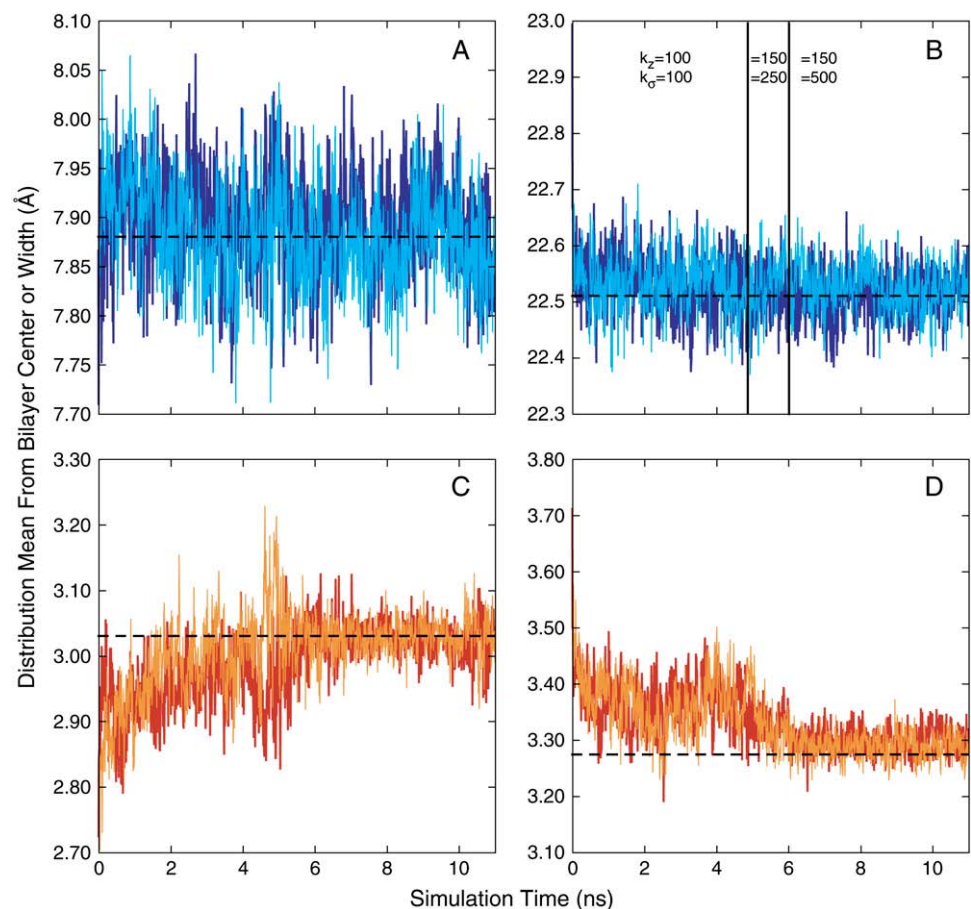


FIGURE 4 Evolution of the double-bond and water group distribution parameters for the pure DOPC bilayer system. The mean positions for the double-bond and water groups are shown in panels *A* and *B*, respectively, with the upper- and lower-leaflet values differentiated by the solid blue and red lines. The absolute value of the lower-leaflet results is shown to place both data sets on the same scale. Similarly, the distribution widths for the double-bond and water groups are shown in panels *C* and *D*, respectively. The target values are indicated by the dashed lines. During the course of the simulation, the force constants on the mean position and width terms of the restraints were increased until the target values were reached. Table 1 gives the final force constant values used. During the first 6 ns, the force constants were adjusted to bring the distribution parameters to their target values, as indicated by the regions separated by vertical bars in panel *B* (though these regions are only shown in *B*, they are the same for all of the panels). After 6 ns, the target distribution values were reached and the remaining 5 ns were used in the analysis of the trajectory.



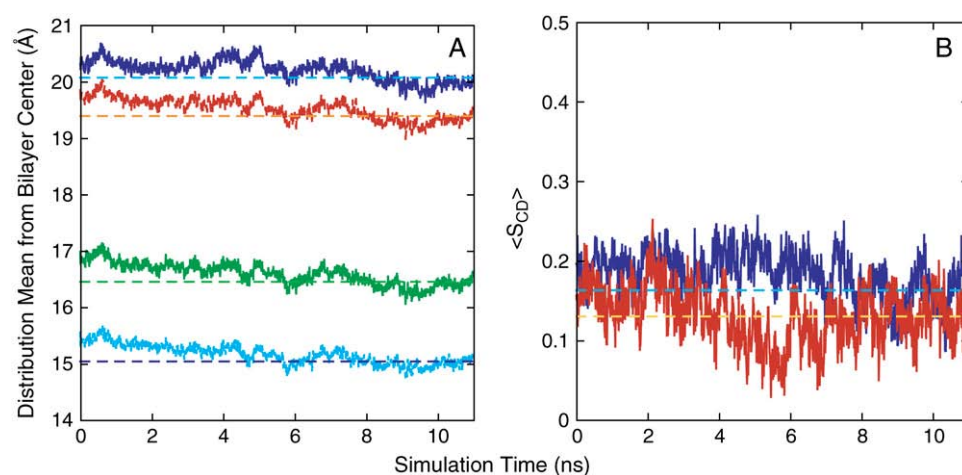


FIGURE 5 Evolution of headgroup component mean positions and deuterium order parameters for lipid chain carbons. (A) Mean positions for the choline (dark blue), phosphate (red), glycerol (green), and carbonyl (light blue) groups are shown. (B) Evolution of the  $\langle S_{CD} \rangle$  for the C6 (blue) and C13 (red) carbons on the lipid tails. The average values from the last 5 ns are indicated by the dashed lines in both panels. Stable mean position and  $\langle S_{CD} \rangle$  values are reached after 6 ns of simulation time.

for each of the systems. The experimental  $d$ -spacing is 49.1 Å, whereas the  $d$ -spacing for the unrestrained system was found to be 50.4 Å (7), which is apparent in the wider, and hence lower, densities, observed in the scattering-length densities profiles. On the other hand, a smaller average  $d$ -spacing of 45.2 Å and a larger area/lipid of 63.3 Å<sup>2</sup> (compared to the experimental value of 59.3 Å<sup>2</sup>) was found for the restrained system (Fig. 7). With a smaller  $d$ -spacing, the restrained

system is more compressed compared to the experimental system, and this is reflected in the observed higher densities. However, the apparent differences between the restrained and experimental neutron profiles, which show relatively good agreement compared to the corresponding x-ray profiles, are due in part to the scattering-length density per lipid scale used here. The differences between the neutron and x-ray profiles will be further addressed below.

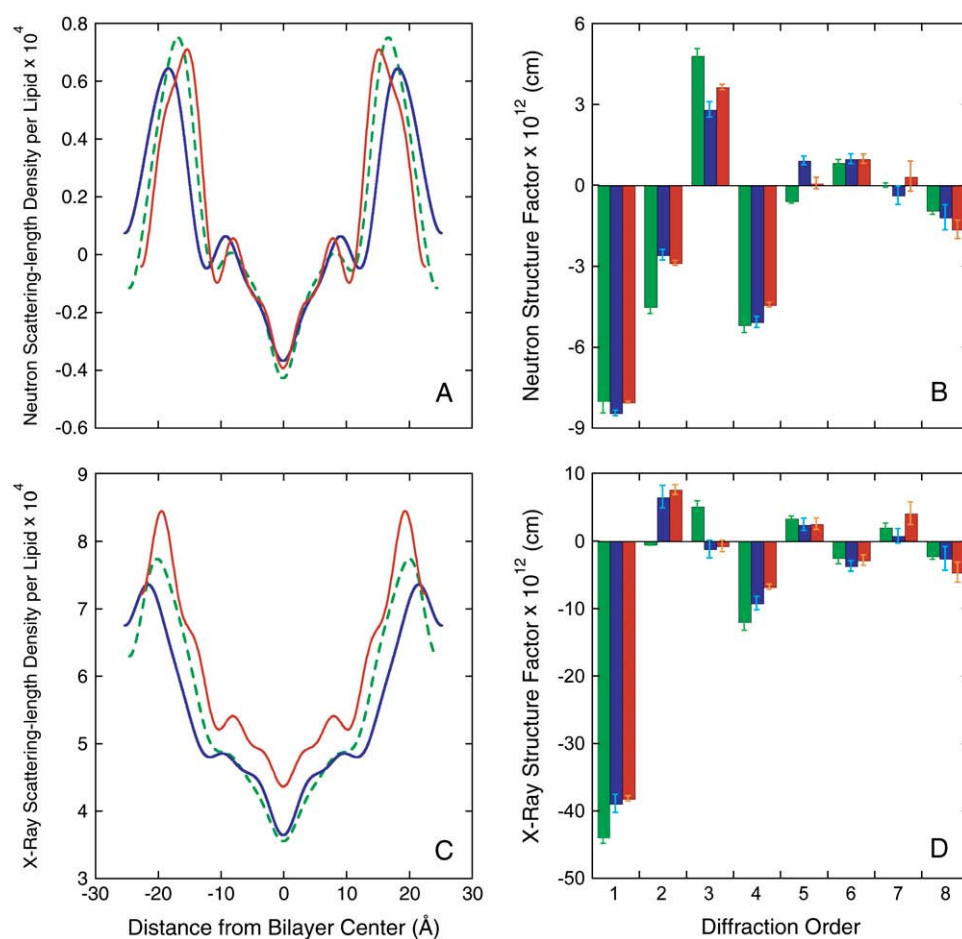


FIGURE 6 Eight-order neutron and x-ray Fourier reconstructed scattering-length density profiles and structure factors for the experimental (green), unrestrained (blue), and restrained (red) pure DOPC system. (A and B) Neutron results. (C and D) X-ray results. The restrained neutron scattering-length density profile shows better agreement with experiment compared to the unrestrained system in both the density profile and the structure factors. The x-ray profile, however, shows more deviations from the experimental profile, due in part to the larger difference in the  $d$ -spacing of the restrained system compared to the experimental system (3.9 Å) compared to the unrestrained system with the experimental system (1.3 Å). Although the x-ray structure factors for both the restrained and unrestrained systems are similar, the differences in the density profiles can also be attributed in part to the difference in their  $d$ -spacings.

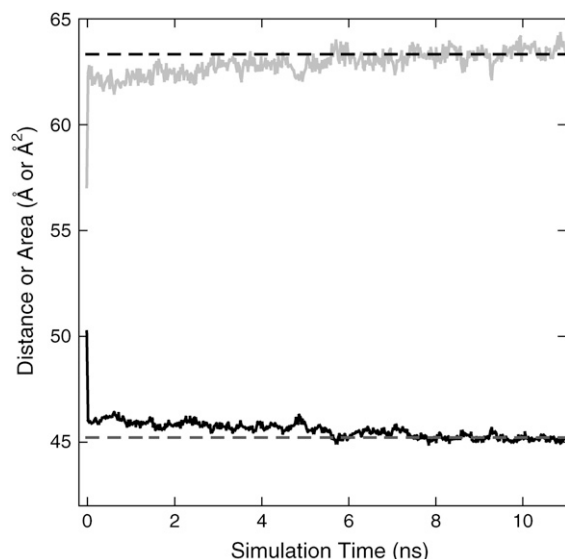


FIGURE 7 Evolution of the  $d$ -spacing and area/lipid for the pure DOPC simulation. With the density restraints applied to the double-bond and water groups, the  $d$ -spacing (black solid line) and area/lipid (gray solid line) initially rapidly change from the starting values, then slowly reach stable values at 6 ns as the rest of the bilayer structure equilibrates. The average values of the last 5 ns of the simulation are indicated by dashed lines.

Fig. 6, *B* and *D*, shows the corresponding structure factors for the neutron and x-ray scattering-length density profiles, respectively. Just as the restrained neutron density profile shows better overall agreement with the experiment compared to the unrestrained system, the 1st-, 2nd-, 3rd-, and 5th-order neutron structure factors of the restrained system also agree better with experiment. In the x-ray data, one can see that most of the restrained and unrestrained structure factors agree within experimental error of each other, but both sets show significant differences compared to the experimental values. Although the structure factors of the restrained and unrestrained x-ray systems are very similar, the main differences in the density profiles can be attributed to the differences in  $d$ -spacing for these two systems.

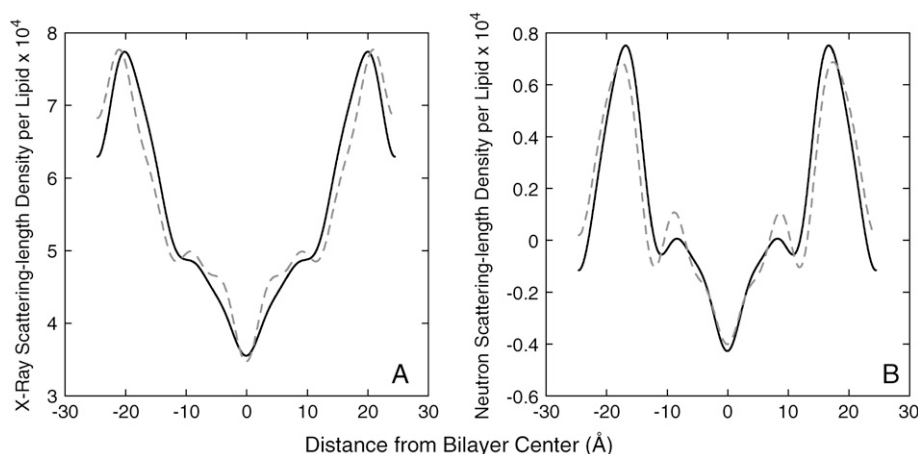


FIGURE 8 Comparison of NVT simulation x-ray and neutron scattering-length density profiles with the experimental profiles. The x-ray profiles are shown in panel *A*, and the neutron profiles are shown in panel *B*, with the solid lines indicating the experimental results and the dashed lines indicating the simulation results. Even when the experimental membrane surface area is used in the simulation, differences between the simulation and experimental profiles are still present.

## Constant-volume simulation

Even with the application of the experiment-based density restraints described here, the large differences observed between the simulation structure factors and scattering-length density profiles with the experimental results for the neat DOPC bilayer (Fig. 6) indicate inadequacies of this force field. A significant structural discrepancy between the restrained simulation and experimental results is the difference in the membrane area/lipid, which was  $63.3 \text{ Å}^2$  in the simulation and  $59.3 \text{ Å}^2$  in the experiment. To investigate how the use of the correct membrane surface area affects the membrane structure, another simulation of the neat DOPC bilayer was performed, but under NVT conditions, using the experimental  $d$ -spacing and area/lipid values for this system determined by Wiener and White (6).

The neutron and x-ray scattering-length density profiles for the NVT simulations and experimental profiles are shown in Fig. 8. The agreement between the constant-volume simulation and the experiment is better than that found between the restrained simulation and experiment, indicating the importance of the area/lipid and  $d$ -spacing values for membrane structure. However, the constant-volume simulation density profiles still show clear differences compared to the experimental profiles. In particular, the simulation neutron profile shows increased density in the region of the double-bonds, and the main interfacial peaks in the x-ray profile are shifted outward, away from the bilayer center. An investigation of the water distribution in the constant-volume simulation provides some insight into the origin of these differences. Fig. 9 shows the water distribution and the corresponding Gaussian fit. The Gaussian distribution parameters compared with the experimental values (6) (Table 2), indicate that the distribution is shifted and is too wide, similar to the results previously obtained for the same system simulated at NPT conditions (7). This diffuse water distribution suggests that proper hydration of the lipid headgroups is not being achieved in the simulations. As the area/lipid for DOPC membranes has been shown to depend on hydration (2,40), an inaccurate water distribution can give rise to an

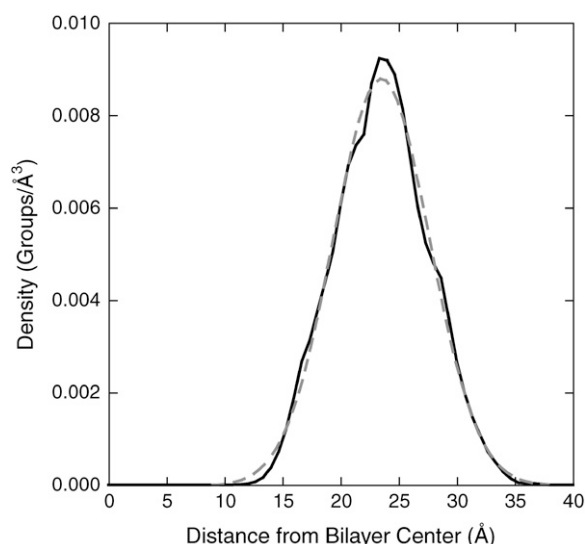


FIGURE 9 Water distribution calculated from the NVT simulation with the corresponding Gaussian fit. The direct simulation results are shown by the black solid line, and the Gaussian fit is shown by the gray dashed line. Based upon the Gaussian fit parameters, given in Table 2, the simulation water distribution is shifted and wider than the experimentally determined distribution.

inaccurate area/lipid and  $d$ -spacing, and is likely the primary reason for the structural discrepancies observed in the simulations.

### DOPC bilayer with melittin

As indicated in Table 1, two restraints were used to restrain the MLT distributions, one for each leaflet, with the restraint group in each leaflet consisting of two MLT peptides. Fig. 10 shows the evolution of mean and width parameters for these restraints as a function of simulation time. As in the case of the pure bilayer restraints, the MLT mean position values rapidly reach the target values, whereas the group standard deviations require more simulation time. However, both the mean position and width values reach their targets within a few nanoseconds.

Although the restraints used for this system were applied to the total MLT distribution in each leaflet (i.e., the distribution of the two MLTs per leaflet), one can also investigate the individual MLT distribution parameters to see how they compare with the total distribution parameters (Fig. 11). For the upper-leaflet MLT parameters (Fig. 11, *A* and *B*), one can see that two MLTs act in a similar manner and mirror the total upper-leaflet parameters. The lower-leaflet param-

eters (Fig. 11, *C* and *D*), however, show that the two MLTs explore different density distributions, indicating that the restraints simply do not “lock-down” the peptides, but rather allow them to explore configuration space independently within the bounds of the restraints.

One of the key aims of the experimental diffraction study on MLT in a DOPC bilayer (16) was to determine the disposition of the peptide in the bilayer. To accomplish this, the x-ray structure factors from the pure DOPC and DOPC + MLT systems were used in a refinement procedure to give the MLT distribution alone. A similar procedure was used to calculate the MLT distribution from the simulations by first calculating the structure factors for the pure DOPC and DOPC + MLT systems. Because only five orders of diffraction were observed experimentally for the DOPC + MLT system, the simulation analyses were also based upon five orders of diffraction. Fig. 12 *A* shows the x-ray scattering-length density profiles for the pure DOPC bilayer (data given in Benz et al. (7)) along with the DOPC + MLT system. As in the experimental results (Fig. 1 *C* of Hristova et al. (16)), the addition of MLT in the simulation perturbs the bilayer structure in a similar manner, though the perturbations are larger in the simulated system. To determine the simulated MLT distribution, the structure factors for the DOPC + MLT system with and without MLT were calculated and the difference structure factors (MLT system with MLT and MLT system without MLT) were inverted to produce the MLT distribution alone (Fig. 12 *B*). Fig. 13 shows an analysis of the structure-factor-reconstructed MLT distribution along with the distributions calculated directly from the atomic positions in the simulation. In Fig. 13 *A*, the structure-factor-based MLT distribution is shown along with a Gaussian fit whose mean position and width parameters are given in Table 3. Fig. 13 *B* shows the MLT density profiles obtained from the atomic coordinates along with the Gaussian fit from Fig. 13 *A*. The mean positions and widths determined from the atomic positions are given in Table 3. Finally, Fig. 13 *C* shows the individual and collective MLT direct distributions in the two leaflets. The structure-factor-reconstructed MLT distribution fits a Gaussian quite well, whereas the direct distributions tend to be slightly thinner and more peaked.

## DISCUSSION

Although simulation force fields are not yet perfect (7), the use of restraints based upon experimental data is an effective way to help simulations sample configurations consistent with experimental data. For bilayer and bilayer-peptide systems, diffraction data can provide a great deal of structural information, and represent a good starting point for defining such restraints. As shown here, molecular component-group-distribution means and widths can be effectively restrained to target values obtained from diffraction experiments, allowing the simulations to make direct contact with the experiments.

TABLE 2 Water distribution parameters

	Mean position (Å)	Distribution width (Å)
Simulation (NVT)	23.52 ± 0.04	5.87 ± 0.06
Experiment	22.51 ± 0.77	4.63 ± 0.48

NVT, constant particle number, volume, and temperature.



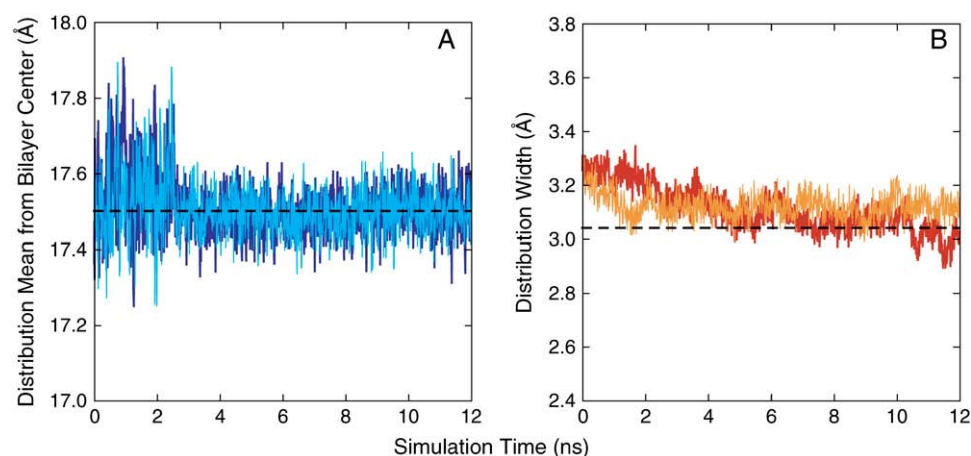


FIGURE 10 Evolution of the distribution mean positions and widths for the two MLT restraint groups. The distribution means are shown in panel A, and the distribution widths in panel B. The upper- and lower-leaflet results are differentiated by the line colors and the dashed lines indicate the target values. The restraint-force constants were not varied over the course of the simulation. After 6 ns, the target distribution values were reached. As with the other simulations reported here, the distribution widths required more time to reach the target values compared to the mean positions.

Although the restraints applied to the pure DOPC bilayer system did not fix all of the structural discrepancies previously observed for the unrestrained simulation of this system compared to experiment (7), improvements in the bilayer structure are seen, particularly in the neutron scattering-length density profiles and in the regions around the restrained groups. The x-ray profile shows more structural differences with the experiment compared to the neutron results, which can in part be attributed to the scattering-

length density per lipid scale, as well as the sensitivity of x-ray profiles to  $d$ -spacing. Because the scaling of these profiles depends both upon the  $d$ -spacing and the per-lipid scattering-length of the components in the system, changes in the  $d$ -spacing will be more apparent for x-ray profiles than for neutron profiles, due to the simple fact that the magnitude of typical x-ray scattering is greater compared to neutron scattering in the scattering-length density per-lipid scale. To illustrate this, Fig. 14 shows the simulation x-ray and neutron

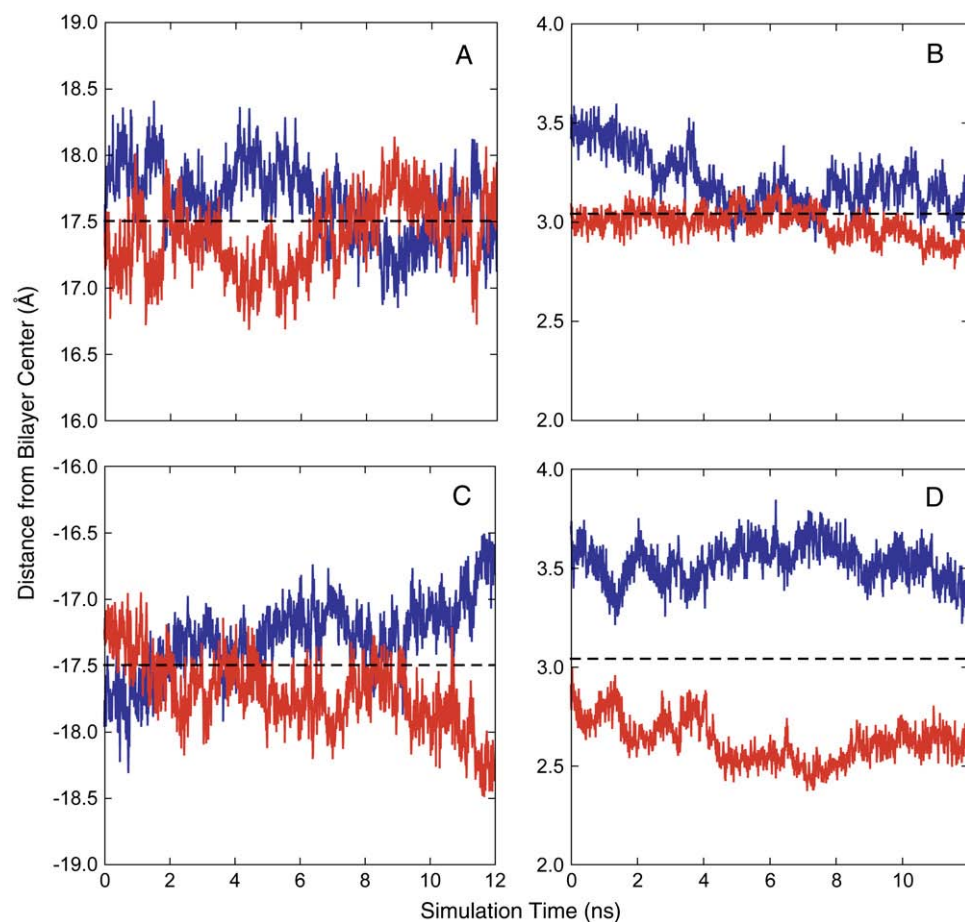


FIGURE 11 Evolution of the individual MLT distribution parameters in each leaflet. In the upper leaflet ((A) distribution mean and (B) distribution width), the two MLT peptides behave similarly (shown separately in blue and red solid lines). In the lower leaflet, however ((C) distribution mean and (D) distribution width), the two MLTs appear to sample slightly different distributions, indicating that the restraints do not simply fix the proteins in the bilayer, but, rather, allow them to explore configuration space within the range determined by the experimentally-derived density distributions. The average values of the parameters are indicated by the dashed lines.

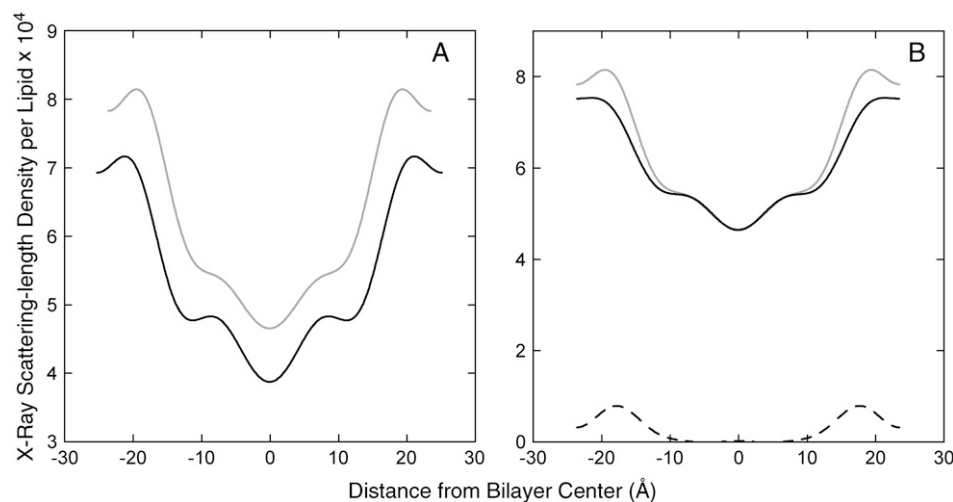


FIGURE 12 Five-order Fourier reconstructions of scattering-length density profiles. (A) Profiles for the pure DOPC bilayer without restraints (black) and the DOPC + MLT system with restraints (gray). (B) Density profiles for the DOPC + MLT system including the MLT contributions (gray) and excluding the MLT contributions (black). The MLT distribution is shown by the black dashed line. Comparison of the DOPC + MLT density with the pure bilayer density in A shows that addition of the peptide to the bilayer perturbs the pure bilayer structure, which was also observed experimentally (15). To determine the MLT distribution from the simulation, the difference structure factors were computed from the DOPC + MLT system with and without the MLT contributions.

scattering-length density profiles, reconstructed using the simulation structure factors at both the simulation and experimental  $d$ -spacing values, compared to the experimental profiles. The simulation neutron profiles show minor differences compared to the more obvious differences between the x-ray profiles.

Another important issue illustrated by the difference in agreement between the neutron and x-ray scattering-length density profiles with the experimental profiles arises from the fact that neutron and x-ray diffraction methods give different views of the bilayer. Close agreement of a simulated x-ray scattering-length density profile alone with the corresponding experimental profile does not necessarily indicate that the simulated bilayer structure itself is in agreement with the actual bilayer structure. As illustrated in the results here, the neutron profile with restraints shows good agreement with the experimental profile, whereas the x-ray profile shows more differences. Though both x-ray and neutron diffraction data are not

always readily available, using both when available can give a more complete picture of the system.

Analysis of the component-group distributions for the pure bilayer system with and without restraints shows that the restraints do in fact bring these distributions into better agreement with the experimental distributions, as indicated in Fig. 4. The observed discrepancies in the scattering-length density profiles can therefore be attributed to the effect the restraints have upon the neighboring groups, and not the restrained groups themselves. The restrained groups induce different packing of the neighboring lipid components compared to the unrestrained simulation, which improves the bilayer structure in some regions and introduces differences, compared to the experiment, in others. It is worth noting that when the restraints are released, the distribution parameters for the double-bond and water groups rapidly return to their pre-restrained values, indicating, in part, that these distributions along with the collective bilayer structure are not compatible

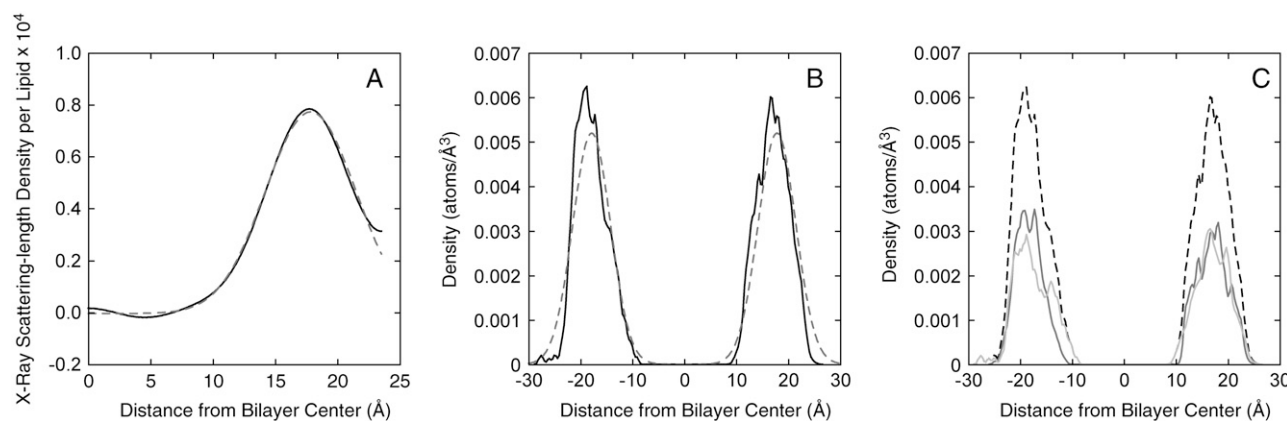


FIGURE 13 Analysis of the MLT distribution. (A) Five-order Fourier-reconstructed distribution (solid line) along with a Gaussian fit (dashed line), which accurately describes the data. (B) Density profiles obtained directly from the simulation (solid lines) are shown along with the Gaussian fit obtained in panel A (dashed lines). There are slight differences in the two views of the MLT distribution, but both are qualitatively the same. Finally (C), the individual MLT distributions (solid lines) are shown with the total MLT distribution (dashed lines). Although the MLT peptides in the lower leaflet appear to sample slightly different distributions, overall, the individual and total distributions are very similar.

**TABLE 3** Melittin distribution parameters

	Mean position (Å)	Distribution width (Å)
Simulation	$17.50 \pm 0.06$	$4.37 \pm 0.08$
Gaussian fit	$17.85 \pm 0.01$	$5.15 \pm 0.03$
Experiment	$17.5 \pm 0.2$	$4.3 \pm 0.4$

with the current force-field parameters. Given future improvements to the force field, however, the restraints described here could be used as a tool to rapidly equilibrate newly constructed systems that differ from the experimental structure.

The analysis of the NVT DOPC bilayer showed that even when the simulation was carried out at the correct surface area, differences in the simulation and experimental density profiles were observed. In particular, the water distribution differed compared to the experimentally determined distribution (6). As water plays an important role in the hydration of the lipid headgroups, these results suggest that force-field refinements to the water or water/headgroup parameters may provide more accurate membrane hydration and would likely affect the total membrane structure. In particular, a more localized water distribution in the interfacial region should increase the area/lipid of a simulated DOPC bilayer at NPT conditions, which currently gives an area/lipid that is too small.

The DOPC + MLT application of the restraint method highlights another useful aspect of the method, namely, that it is a useful approach to rapidly equilibrate newly constructed membrane-peptide systems into states consistent with experimental results. Aside from orienting the hydrophobic faces of the helices toward the hydrocarbon region of the bilayer and positioning the helices so as to avoid direct interactions with one another, little additional work was used to set up the initial configuration of MLT in the DOPC

bilayer. Rather, the restraints were simply applied and the system was allowed to explore configuration space under their influence. Furthermore, the restraints do not simply fix the proteins in the bilayer, exhibited by the differences in the behavior of the mean and standard deviation values among the individual MLT proteins (Fig. 11). However, the collective distributions are in agreement with the experimental parameters, consistent with the idea of the diffraction experiment revealing the ensemble average. This is important for addressing questions about the ways in which MLT perturbs the bilayer structure.

The MLT distributions determined from the atomic positions and the Fourier reconstruction closely approximate the experimental distribution (Fig. 13, Table 3). Although the restraints do not explicitly enforce a Gaussian distribution (only the distribution mean position and width are restrained), the Fourier reconstructed MLT distribution is found to be accurately modeled by a Gaussian (Fig. 13 A), as for the experimental data. Comparison of the MLT distributions computed directly from the trajectory with the Gaussian fit reveals some differences, namely, a slightly shifted mean position and larger width for the fit (Fig. 13 B). As is apparent in the snapshot from Fig. 1, and as observed over the course of the simulation, kinks were found in two of the peptides, whereas the other two remained helical. This is not unexpected, because as Hrivtova et al. (16) noted, MLT must adopt many different conformations in the interface. The helical and kinked structures observed in the NPT simulation thus suggest the kinds of configurations that might exist in the experimental ensemble of peptides. A more detailed analysis of the MLT system will be given in a subsequent article.

Although one could in principle restrain an entire system given the availability of enough experimental component-group distribution parameters, the real motivation for

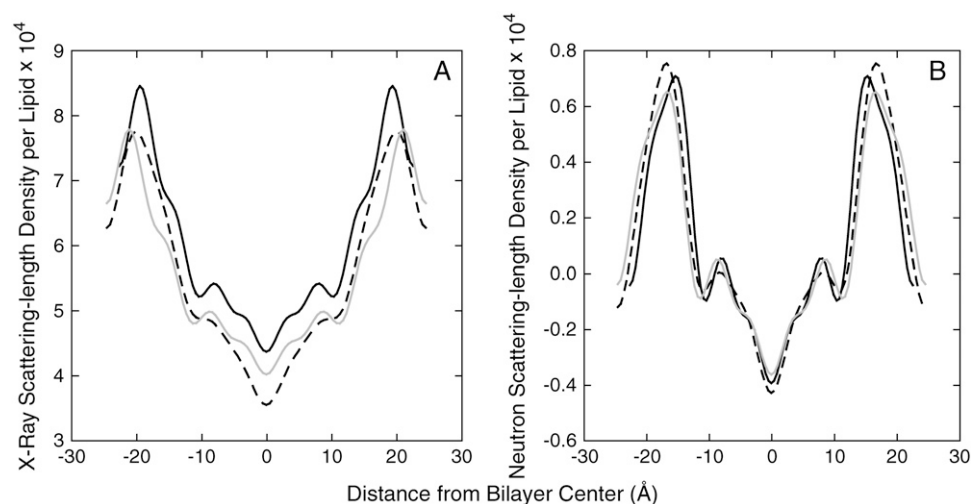


**FIGURE 14** Comparison of simulation x-ray and neutron scattering-length density profiles reconstructed at the simulation and experimental  $d$ -spacing values, with experimental profiles. (A) X-ray simulation profile reconstructed at the simulation  $d$ -spacing (45.2 Å, dark gray solid line) shows more differences with the same reconstruction at the experimental  $d$ -spacing (49.1, gray solid line), compared to the corresponding neutron reconstructions from the simulation data in panel B (simulation  $d$ -spacing, dark gray solid line; experimental  $d$ -spacing, gray solid line). In both panels, the experimental profile is shown by the dashed line for reference. These profiles illustrate the increased sensitivity of x-ray scattering-length densities to  $d$ -spacing, compared to neutron scattering-length densities on the per-lipid scale.

developing and using the density-based restraints presented here is to apply them to a small number of key groups for which experimental distribution parameters are easily measured, allowing the simulation trajectories to explore configurations consistent with the experimentally derived distributions. The use of the diffraction-based density restraints are anticipated to be especially helpful for rapid equilibration of a system into experimentally valid configurations, after which the restraints could be removed and the system allowed to evolve naturally. In short, the restraint method described here constitutes a simulation-based approach for generating three-dimensional structures from one-dimensional diffraction data on membrane systems.

The NAMD software was developed by the Theoretical and Computational Biophysics Group at the Beckman Institute for Advanced Science and Technology at the University of Illinois at Urbana-Champaign.

This research was supported in part by National Science Foundation grant CHE-0417158 to D.J.T., National Institutes of Health grants GM68002, RR14812, and GM46823 to S.H.W., and by National Research Service Award 5 T15 LM00744 from the National Library of Medicine to R.W.B.

## REFERENCES

- McIntosh, T. J. 1990. X-ray diffraction analysis of membrane lipids. In *Molecular Description of Biological Membrane by Computer Aided Conformational Analysis*. R. Brasseur, editor. CRC Press. Boca Raton, FL. 241–266.
- Tristram-Nagle, S., H. I. Petrache, and J. F. Nagle. 1998. Structure and interactions of fully hydrated dioleoylphosphatidylcholine bilayers. *Biophys. J.* 75:917–925.
- White, S. H., and M. C. Wiener. 1995. Determination of the structure of fluid lipid bilayer membranes. In *Permeability and Stability of Lipid Bilayers*. E. A. Disalvo and S. A. Simon, editors. CRC Press. Boca Raton, FL. 1–19.
- Wiener, M. C., and S. H. White. 1991. Fluid bilayer structure determination by the combined use of x-ray and neutron diffraction. I. Fluid bilayer models and the limits of resolution. *Biophys. J.* 59: 162–173.
- Franks, N. P., and Y. K. Levine. 1981. Low-angle X-ray diffraction. In *Membrane Spectroscopy*. E. Grell, editor. Springer-Verlag. Berlin, Germany. 437–487.
- Wiener, M. C., and S. H. White. 1992. Structure of a fluid dioleoylphosphatidylcholine bilayer determined by joint refinement of x-ray and neutron diffraction data. III. Complete structure. *Biophys. J.* 61:434–447.
- Benz, R. W., F. Castro-Román, D. J. Tobias, and S. H. White. 2005. Experimental validation of molecular dynamics simulations of lipid bilayers: a new approach. *Biophys. J.* 88:805–817.
- Franks, N. P., T. Arunachalam, and E. Caspi. 1978. A direct method for determination of membrane electron density profiles on an absolute scale. *Nature*. 276:530–532.
- Wiener, M. C., and S. H. White. 1991. Transbilayer distribution of bromine in fluid bilayers containing a specifically brominated analog of dioleoylphosphatidylcholine. *Biochemistry*. 30:6997–7008.
- Büldt, G., H. U. Gally, A. Seelig, J. Seelig, and G. Zaccari. 1978. Neutron diffraction studies on selectively deuterated phospholipid bilayers. *Nature*. 271:182–184.
- Wiener, M. C., G. I. King, and S. H. White. 1991. Structure of a fluid dioleoylphosphatidylcholine bilayer determined by joint refinement of x-ray and neutron diffraction data. I. Scaling of neutron data and the distribution of double-bonds and water. *Biophys. J.* 60:568–576.
- Wiener, M. C., and S. H. White. 1992. Structure of a fluid dioleoylphosphatidylcholine bilayer determined by joint refinement of x-ray and neutron diffraction data. II. Distribution and packing of terminal methyl groups. *Biophys. J.* 61:428–433.
- Jacobs, R. E., and S. H. White. 1989. The nature of the hydrophobic binding of small peptides at the bilayer interface: implications for the insertion of transbilayer helices. *Biochemistry*. 28:3421–3437.
- Bradshaw, J. P., S. M. A. Davies, and T. Hauss. 1998. Interaction of substance P with phospholipid bilayers: a neutron diffraction study. *Biophys. J.* 75:889–895.
- Hristova, K., W. C. Wimley, V. K. Mishra, G. M. Anantharamaiah, J. P. Segrest, and S. H. White. 1999. An amphipathic  $\alpha$ -helix at a membrane interface: A structural study using a novel x-ray diffraction method. *J. Mol. Biol.* 290:99–117.
- Hristova, K., C. E. Dempsey, and S. H. White. 2001. Structure, location, and lipid perturbations of melittin at the membrane interface. *Biophys. J.* 80:801–811.
- Bassolino-Klimas, D., R. Tejero, S. R. Krystek, W. J. Metzler, G. T. Montelione, and R. E. Bruccoleri. 1996. Simulated annealing with restrained molecular dynamics using a flexible restraint potential: theory and evaluation with simulated NMR constraints. *Protein Sci.* 5:593–603.
- Brünger, A. T., G. M. Clore, A. M. Gronenborn, and M. Karplus. 1986. Three-dimensional structure of proteins determined by molecular dynamics with interproton distance restraints: application to crambin. *Proc. Natl. Acad. Sci. USA*. 83:3801–3805.
- Kaptein, R., E. R. P. Zuiderweg, R. M. Scheek, R. Boelens, and W. F. van Gunsteren. 1985. A protein structure from nuclear magnetic resonance data: lac repressor headpiece. *J. Mol. Biol.* 182:179–182.
- Park, S., F. Khalili-Araghi, E. Tajkhorshid, and K. Schulten. 2003. Free energy calculation from steered molecular dynamics simulations using Jarzynski's equality. *J. Chem. Phys.* 119:3559–3566.
- Roux, B. 1995. The calculation of the potential of mean force using computer simulations. *Comput. Phys. Commun.* 91:275–282.
- Souaille, M., and B. Roux. 2001. Extension to the weighted histogram analysis methods: combining umbrella sampling with free energy calculations. *Comput. Phys. Commun.* 135:40–57.
- Nagle, J. F., and S. Tristram-Nagle. 2001. Structure of lipid bilayers. *Biochim. Biophys. Acta*. 1469:159–195.
- Kalé, L., R. Skeel, M. Bhandarkar, R. Brunner, A. Gursoy, N. Krawetz, J. Phillips, A. Shinozaki, K. Varadarajan, and K. Schulten. 1999. NAMD2: greater scalability for parallel molecular dynamics. *J. Comput. Phys.* 151:283–312.
- Schlenkrich, M., J. Brickmann, A. D. MacKerell, Jr., and M. Karplus. 1996. An empirical potential energy function for phospholipids: criteria for parameter optimization and applications. In *Biological Membranes*. K. M. Merz, Jr., and B. Roux, editors. Birkhäuser. Boston, MA. 31–81.
- Feller, S. E., D. X. Yin, R. W. Pastor, and A. D. MacKerell, Jr. 1997. Molecular dynamics simulation of unsaturated lipid bilayers at low hydration: parameterization and comparison with diffraction studies. *Biophys. J.* 73:2269–2279.
- Feller, S. E., and A. D. MacKerell, Jr. 2000. An improved empirical potential energy function for molecular simulations of phospholipids. *J. Phys. Chem. B*. 104:7510–7515.
- Maitland, G. C. 1981. *Intermolecular Forces: Their Origin and Determination*. Clarendon Press, New York, NY and Oxford, UK.
- Tu, K., D. J. Tobias, and M. L. Klein. 1995. Constant pressure and temperature molecular dynamics simulation of a fully hydrated liquid crystal phase dipalmitoylphosphatidylcholine bilayer. *Biophys. J.* 69:2558–2562.
- Feller, S. E., Y. Zhang, R. W. Pastor, and B. R. Brooks. 1995. Constant pressure molecular dynamics simulation: the Langevin piston method. *J. Chem. Phys.* 103:4613–4621.
- Essmann, U., L. Perera, M. L. Berkowitz, T. Darden, H. Lee, and L. G. Pedersen. 1995. A smooth particle mesh Ewald method. *J. Chem. Phys.* 103:8577–8593.

32. Tuckerman, M., and B. J. Berne. 1992. Reversible multiple time scale molecular dynamics. *J. Chem. Phys.* 97:1990–2001.
33. Grubmüller, H., H. Heller, A. Windemuth, and K. Schulten. 1991. Generalized Verlet algorithm for efficient molecular dynamics simulations with long-range interactions. *Mol. Simul.* 6:121–142.
34. Humphrey, W., W. Dalke, and K. Schulten. 1996. VMD: visual molecular dynamics. *J. Mol. Graph.* 14:33–38.
35. Mashl, R. J., H. L. Scott, S. Subramaniam, and E. Jakobsson. 2001. Molecular simulation of dioleoylphosphatidylcholine lipid bilayers at differing levels of hydration. *Biophys. J.* 81:3005–3015.
36. Bernèche, S., M. Nina, and B. Roux. 1998. Molecular dynamics simulation of melittin in a dimyristoylphosphatidylcholine bilayer membrane. *Biophys. J.* 75:1603–1618.
37. Bachar, M., and O. M. Becker. 1999. Melittin at a membrane/water interface: effects on water orientation and water penetration. *J. Chem. Phys.* 111:8672–8685.
38. Bachar, M., and O. M. Becker. 2000. Protein-induced membrane disorder: a molecular dynamics study of melittin in a dipalmitoylphosphatidylcholine bilayer. *Biophys. J.* 78:1359–1375.
39. Lin, J.-H., and A. Baumgärtner. 2000. Adsorption of melittin to a lipid bilayer: a molecular dynamics study. *J. Mol. Liquids.* 84: 89–98.
40. Hristova, K., and S. H. White. 1998. Determination of the hydrocarbon core structure of fluid dioleoylphosphocholine (DOPC) bilayers by x-ray diffraction using specific bromination of the double-bonds: effect of hydration. *Biophys. J.* 74:2419–2433.